Light: Science & Applications (2015) 4, e251; doi:10.1038/lsa.2015.24
© 2015 CIOMP. All rights reserved 2047-7538/15
www.nature.com/lsa

ORIGINAL ARTICLE

Carrier multiplication in germanium nanocrystals

Saba Saeed[1], Chris de Weerd[1], Peter Stallinga[1,2], Frank CM Spoor[3], Arjan J Houtepen[3], Laurens DA Siebbeles[3] and Tom Gregorkiewicz[1]

Carrier multiplication is demonstrated in a solid-state dispersion of germanium nanocrystals in a silicon–dioxide matrix. This is performed by comparing ultrafast photo-induced absorption transients at different pump photon energies below and above the threshold energy for this process. The average germanium nanocrystal size is approximately 5–6 nm, as inferred from photoluminescence and Raman spectra. A carrier multiplication efficiency of approximately 190% is measured for photo-excitation at 2.8 times the optical bandgap of germanium nanocrystals, deduced from their photoluminescence spectra.
Light: Science & Applications (2015) **4,** e251; doi:10.1038/lsa.2015.24; published online 13 February 2015

Keywords: carrier multiplication; germanium nanocrystals; transient absorption

INTRODUCTION

Carrier multiplication (CM) is the phenomenon of the creation of multiple electron–hole (e–h) pairs in semiconductors upon the absorption of a single photon. CM attracts considerable interest because it can enhance performance of the currently available solar cells[1–5] and photo-detectors.[6] Conventionally, these devices operate on a single-photon-to-single-electron conversion basis. In that case, high-energy photons create energetic e–h pairs that cool down first before they are extracted in the form of electric current; i.e., a significant part of the incident light power is converted into heat. The CM phenomenon reduces the amount of energy lost to heat by generating additional free carriers. The charges can be extracted either directly or through the emission of photons of lower energy. In particular, for solar cells, an overall increased efficiency can be expected (up to 44%[2]) for devices that utilize CM. Indeed, quantum efficiencies—defined as the number of e–h pairs generated per absorbed photon—exceeding 100% have been observed,[7] proving the usefulness and feasibility of CM.

CM was first observed in classical crystalline bulk semiconductors, for instance silicon.[8] In bulk materials, CM proceeds *via* impact ionization[9] by hot carriers and its efficiency is relatively low due to competition from the highly effective carrier-cooling process (see Figure 1 for a schematic illustration). An external quantum efficiency—defined as the number of e–h pairs extracted from the device for every absorbed photon—of 170% was observed for photons with energies equal to 6 times the bandgap in bulk germanium.[10] An efficiency of 130% for the generation of an e–h pair by an absorbed photon has been reported for bulk silicon irradiated with ultraviolet light.[8] CM was found to be considerably enhanced in spatially confined materials, such as graphene[11] and lead sulfide nanosheets[12] (two-dimensional confinement), carbon nanotubes[13] and lead selenide nanorods[14,15] (one-dimensional confinement) and in quantum dots (zero-dimensional confinement).[16] In the latter case, CM was studied for quantum dots in a colloidal dispersion or embedded in a solid matrix.[16–18] Generally, in spatially confined materials, the Coulomb interaction between carriers is increased, thereby enhancing charge scattering processes such as CM and Auger recombination. Therefore, the stronger the confinement, the more efficient is the CM process.[19] Moreover, apart from widening the electronic bandgap (in silicon scaling with the square of the diameter[20]), the same quantum confinement relaxes the momentum conservation requirement in optical transitions through Heisenberg's uncertainty relation, thus considerably enhancing the probability of band-to-band transitions for indirect bandgap materials (such as silicon and germanium), lowering the radiative recombination time constant down to the 10-ms range. This relaxation of momentum conservation also enhances CM and Auger recombination.[3]

Past research has demonstrated CM in nanocrystals (NCs) of many semiconductor materials, including lead selenide, lead sulfide, lead telluride, cadmium selenide, indium arsenide, indium phosphide and silicon (see Refs. 1 and 16 and references therein). The identification of CM in silicon NCs was of particular significance in view of the technological importance of silicon and its leading role in the electronics industry.[21] CM in germanium NCs has not been reported until now. Germanium is of interest because it features unique properties, such as extreme chemical purity, a great multiplicity of isotopes, a unique band structure with close values of direct and indirect bandgaps, and a high sensitivity to stress, among others. Moreover, the technical importance of germanium is growing, with applications for detectors[22] and photovoltaics—not only for substrates but also as an active material for tandem cells. The bandgap of (bulk) germanium, 0.67 eV, is nearly ideal for the exploitation of CM in solar cells. The aforementioned theoretical 44% maximum efficiency of solar cells calculated by Nozik[2] is for semiconductors with bandgaps in the range of 0.6–1.0 eV, which is within reach of germanium NCs.

[1]Van der Waals-Zeeman Institute, University of Amsterdam, 1098 XH Amsterdam, The Netherlands; [2]FCT-DEEI, University of the Algarve, 8005-139 Faro, Portugal and [3]Optoelectronic Materials, Faculty of Applied Sciences, Delft University of Technology, 2628 BL Delft, The Netherlands
Correspondence: T Gregorkiewicz, Van der Waals-Zeeman Institute, University of Amsterdam, Science Park 904, 1098 XH Amsterdam, The Netherlands
E-mail: T.Gregorkiewicz@uva.nl
Received 19 July 2014; revised 4 December 2014; accepted 14 December 2014; accepted article preview online 18 December 2014

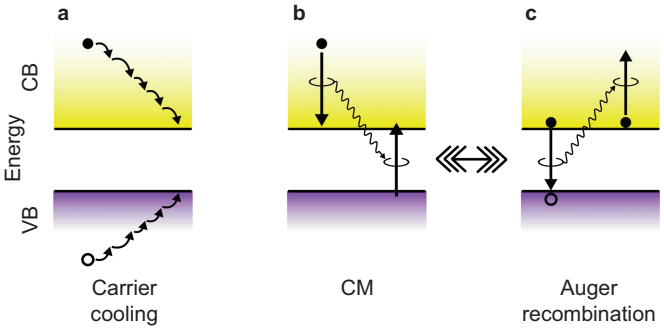

Figure 1 Schematic illustration of the processes described in this work. Upon the absorption of a high-energy photon, an energetic e–h pair is created. (**a**) These electrons and holes can 'cool down' to the band edges in a multistep phonon emission process and can then be extracted in the form of electric current or can recombine either radiatively (emission of a photon with energy equal to the bandgap) or non-radiatively. (**b**) Alternatively, CM can occur, and the 'excess' energy is used to excite a second e–h pair (for simplicity, only electrons are shown, although both electrons and holes can take part in CM). This process can take place when the energy of the electron or the hole is larger than the bandgap. (**c**) The opposite process is Auger recombination, in which the electron recombines with the hole and the released energy is used to excite (a) carrier(s) further into the band. Because of the rapid occurrence of these two processes, one can imagine a superposition state, indicated by the feathered arrow. CB, conduction band; CM, carrier multiplication; e–h, electron–hole; VB, valence band.

In this work, we report the observation of CM in germanium NCs by ultrafast transient absorption (TA) spectroscopy. The measured lifetime of the multiple carriers generated in the process is in the range of tens to hundreds of picoseconds, which is typical for NCs with a diameter of a few nanometers.[13]

MATERIALS AND METHODS

Germanium NCs embedded in a silicon–dioxide matrix were prepared by radiofrequency cosputtering using a multitarget chamber. The thickness of the films was approximately 500 nm, and the germanium content was 20%. The procedure adopted for sample preparation was similar to that described in Refs. 23 and 24. Following deposition, the sputtered layers were annealed in a nitrogen atmosphere at a temperature of 1100 ℃ for 30 min. During the annealing step, the germanium segregates into small crystalline inclusions embedded in a silicon–dioxide matrix.

Measurements of photoluminescence (PL) spectra were performed under continuous-wave excitation with an Nd:YVO_4 laser (Millennia IIs laser system; Spectra Physics, Santa Clara, CA, USA) operating at 532 nm. The PL signal was recorded with a 1 m f/8 monochromator (Jobin-Yvon THR-1000; HORIBA Jobin Yvon, Palaiseau, France) coupled to an infrared germanium detector (Edinburgh Instruments Ltd., Kirkton Campus, Livingston, UK) with a DSP (digital signal processing) lock-in amplifier (Signal Recovery SR7265; Signal Recovery, Oak Ridge, TN, USA). The results were corrected for the spectral response of the system. A Perkin Elmer Lambda 950 ultraviolet-visible-near-infrared spectrometer was used to measure the linear absorption of the sample, with tungsten-halogen and deuterium lamps in combination with a photomultiplier tube and a Peltier-cooled lead sulfide detector providing a detection range of λ_{det}=175–3300 nm. To avoid contributions of the substrate to the data obtained with this setup, the signal of a bare substrate was separately measured and subtracted. An integrating sphere was incorporated to account for scattering effects. Raman spectroscopy with the excitation wavelength of 514.5 nm was used to characterize the nature of the chemical bonds in the sample.

In the TA experiment, the absorption of the system in an excited state induced by a short pump laser pulse is probed and compared to the absorption in the ground state (without the pump pulse). In this way, information on the (time-dependent) concentration of free carriers generated by the pump pulse is obtained. The experimental set-up is described elsewhere;[25] the repetition rate of the (pump) laser pulses was 2.5 kHz and the probe pulse consisted of white light that was spectrally resolved before reaching the detector. The TA signal is defined as the difference of the optical density (OD) of the excited state and the ground state and is obtained as follows:

$$\Delta \mathrm{OD}(\lambda,t) = \log_{10}\left[\frac{I_{\mathrm{off}}(\lambda)}{I_{\mathrm{on}}(\lambda,t)}\right] \quad (1)$$

where I_{off} (I_{on}) is the transmitted probe fluence with the pump laser off (on).

RESULTS AND DISCUSSION

The germanium NCs were optically characterized by measuring the steady-state absorption and PL spectra, which are shown in Figure 2a. The location of the maximum of the PL spectrum implies an optical bandgap of 1.25 eV, which, according to theoretical calculations, corresponds to an average NC diameter of 4–5 nm.[26–28] Nevertheless, there are clear discrepancies in the theoretical modeling and experimental results concerning germanium NCs, and therefore, no well-established generally accepted relationship between germanium NC size and optical bandgap exists.[26–30] In particular Takeoka *et al.*[23] reports that a PL energy of 1.25 eV corresponds to a relatively small NC diameter of ~2 nm, whereas Niquet *et al.*[28] reports the formation of much larger germanium NCs with diameters of ~8 nm upon annealing at the same temperature. However, it is unclear whether the amount of excess germanium and/or sputtering conditions were similar in these two studies. On the theoretical side, Barbagiovanni *et al.*[26] provide a comparison between calculations for weak/medium and strong confinement regimes that agree nicely with the experimental results obtained by Takeoka *et al.*[23] and us, respectively.

The average NC diameter can also be estimated from the width and/or shift of the Raman spectrum (Figure 2b). A shift of the Raman peak appears due to the presence of quantum confinement[31] but also due to stress in the system.[32] The experimentally measured shift implies a germanium NC size of 2 nm. However, the value of the experimentally measured width of the Raman peak corresponds to a germanium NC diameter of ~6 nm,[33] which agrees with the size inferred from the PL according to theoretical calculations. We judge that it is likely that the measured shift in the investigated material is due to the presence of stress, and therefore, we assume that the average size of germanium NCs in the investigated material is approximately 5–6 nm.

We also note that the onset of the optical absorption is at a photon energy lower than the onset of the PL, as seen from Figure 2a. The origin of this low-energy parasitic absorption is yet unclear. It could be due to the presence of large NCs that do not contribute to emission, or it could be due to the formation of electronic states within the bandgap of the NCs. In either case, these features would appear in the steady-state absorption as well as in the TA measurements but not in the PL spectrum.

Figure 3 shows the TA (OD *vs.* t) measured around a below-bandgap probe wavelength of λ=1300 nm (obtained by integrating the signal from 1200 nm to 1400 nm) for two excitation pump wavelengths: λ^*=800 nm (Figure 3a) and λ^*=400 nm (Figure 3b) (see Supplementary Fig. S1 for the TA data obtained in this study). The TA features a brief bleaching followed by a slower positive component.

doi:10.1038/lsa.2015.24

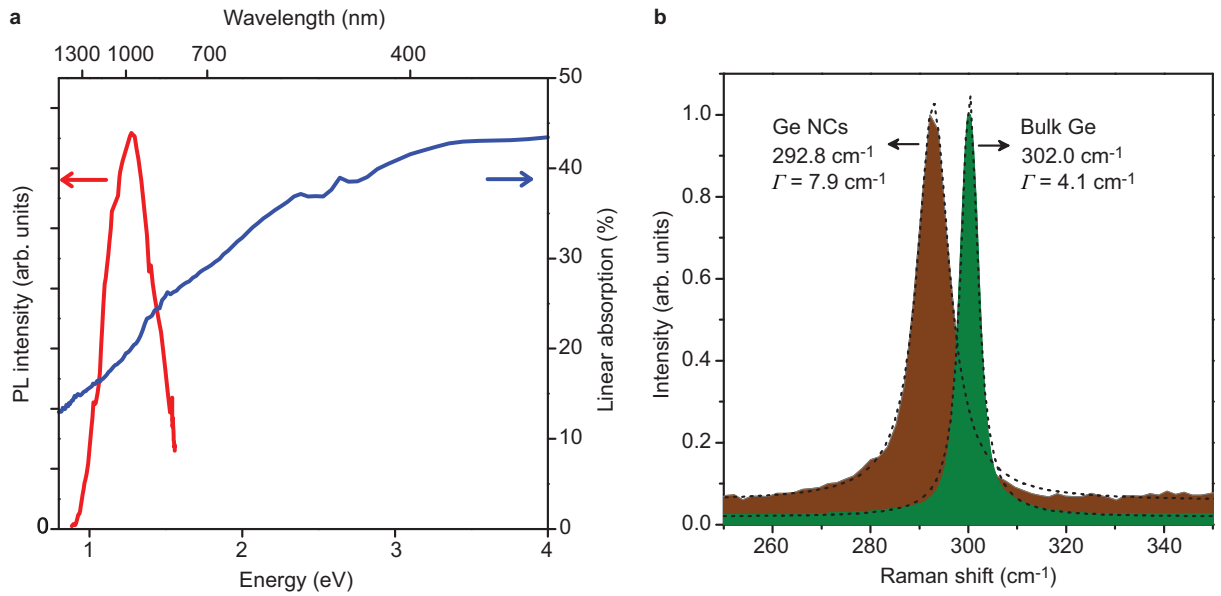

Figure 2 (**a**) Absorption (blue) and PL (red) curves. (**b**) Raman spectrum (brown) with a Lorentzian fit (dashed line) giving the position and width as indicated. For comparison, the bulk germanium spectrum is shown in green. The shift of the peak is due to quantum confinement.[25] NC, nanocrystal; PL, photoluminescence.

The initial negative signal is not understood at present. Additionally, such a negative signal has not been previously observed for Si NCs[34] prepared in a similar way. In the case of silicon NCs, no sub-bandgap absorption was observed; therefore, we can tentatively attribute the measured negative signal to the absorption below the optical bandgap of germanium NCs. In the present case, the initial bleaching of the optical absorption disappears after approximately 20 ps. This is similar to results obtained previously for a similar type of material.[35] The TA signal at longer times is attributed to intraband absorption and is proportional to the density of excited carriers in the entire band, independent of their energy.

We note that the TA behaviors at the two excitation wavelengths are remarkably different. Both show a tail with a long relaxation time compared to the time window (>1 ns). However, for the short-wavelength excitation, the absorption transient has an additional fast component on a timescale of 100 ps. This is the fingerprint of CM, as will now be discussed. In this study, we follow the reasoning of Schaller *et al.*[36] and Trinh *et al.*[37] and summarized by Smith and Binks.[16] The long tail TA is due to NCs containing a single exciton. In the experimental procedure, we ensured operation in the low-fluence regime, so that the average number of absorbed photons (and thus excitons per NC) is very small, $\langle N \rangle \ll 1$. The initial exciton multiplicity directly

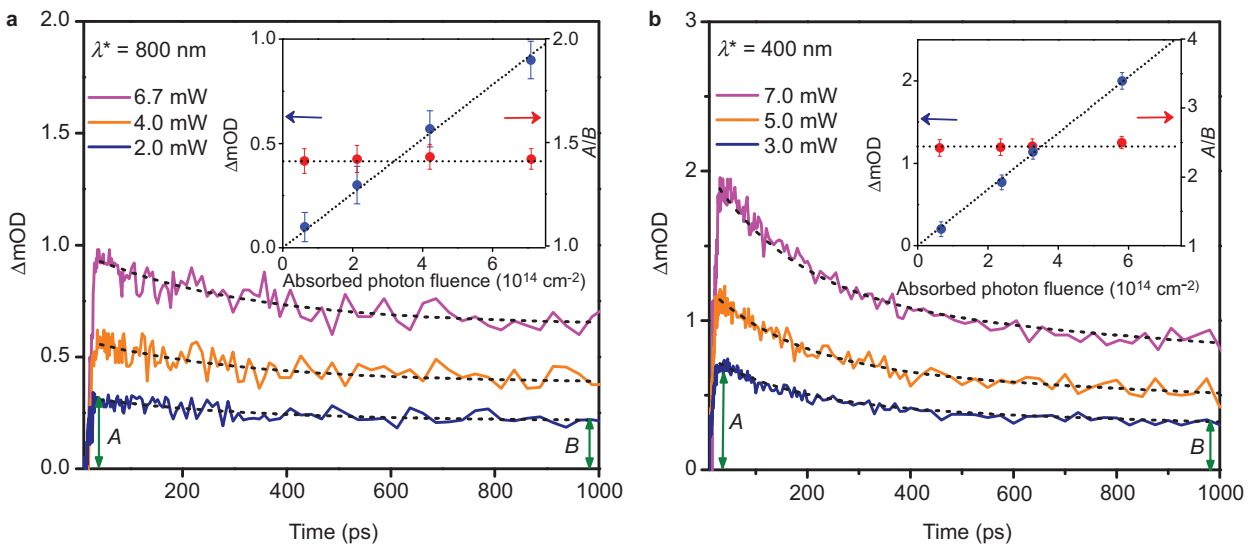

Figure 3 Transient absorption dynamics measured at probe wavelengths λ near 1300 nm (obtained by integrating the signal from 1200 nm to 1400 nm) for excitation wavelengths of $\lambda^*=800$ nm (**a**) and $\lambda^*=400$ nm (**b**) for three different pump pulse fluences and demonstrating the single-photon-absorption regime. The dashed lines are single- (**a**) and double-exponential (**b**) fits to the data. The double-exponential decay at the $\lambda^*=400$ nm excitation wavelength is the fingerprint of CM. The insets show the maximum amplitude of the TA transients (*A*) and its ratio to the amplitude of the single exciton decay tail (*A*/*B*) as a function of the absorbed photons fluence (see text for explanation). CM, carrier multiplication; OD, optical density; TA, transient absorption.

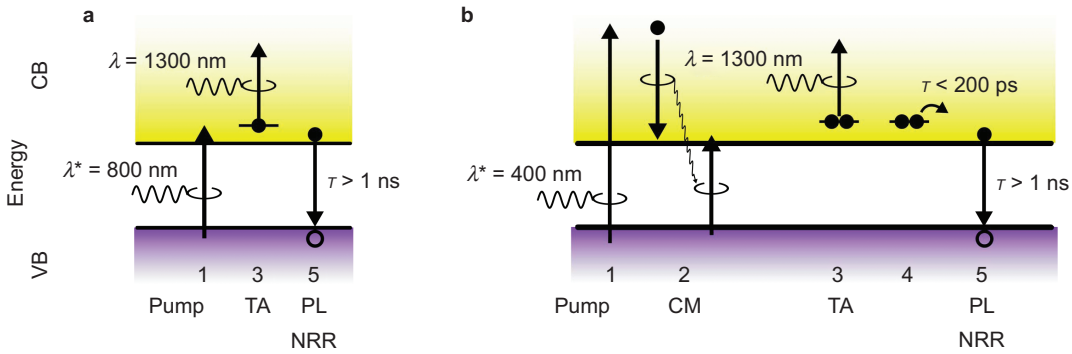

Figure 4 Difference between low pump photon energy (**a**) and high pump photon energy experiments (**b**). e–h pairs produced by a low pump photon energy (1) give rise to a long lived TA (3) and eventually decay *via* PL or NRR (5). For high pump photon energy (1), CM takes place (2), doubling the TA (3). Auger recombination causes the system to rapidly (<200 ps) decay to a single e-h pair (4). The single e–h pair decays *via* PL/NRR (5) as in (**b**). CB, conduction band; CM, carrier multiplication; e–h, electron–hole; NRR, non-radiative recombination; PL, photoluminescence; TA, transient absorption; VB, valence band.

after photo-excitation (and prior to CM) is, in this case, approximately $N_x=1$, meaning that each excited NCs initially contains only one exciton. Under these conditions, most of the NCs are not excited and do not contribute to the TA signal. The TA eventually decays on a timescale exceeding a nanosecond, as the total number of excitons decreases by radiative (PL) and non-radiative recombination (see Figure 4 for a schematic illustration). In the case of short-wavelength high-photon-energy excitation, the hot carriers can induce CM. A single hot e–h pair decays by CM to yield two (or more) e–h pairs at a lower energy (see step 2 in Figure 4b). The time scale of this conversion process is estimated to be 0.1–1 ps.[38–40] Consequently, the amplitude of the TA signal is increased by the higher exciton multiplicity (see step 3 in Figure 4b). This multiple-exciton state, however, is relatively short lived and decays through Auger recombination. Therefore, in the assumed approach, the exciton multiplicity can be estimated by comparing the TA dynamics obtained at a particular excitation energy with the single exciton dynamics;[36,37] this is most easily done by taking the ratio of the initial TA magnitude A, wherein multiple excitons might have been generated, to the magnitude B at a later time when (eventually) the Auger decay is completed. This A/B ratio is shown in both panels of Figure 3.

To ensure that the measurements are conducted in the regime with single photon absorption per NC and to avoid multiple photon absorption per NC per pulse—which would obviously create multiple excitons per NC without the CM effect—our experimental procedure was to reduce the pump pulse intensity until the TA transients (OD *vs.* t) remained invariant. This is illustrated in Figure 3, where the TA dynamics measured for several pump pulse fluences (defined as the number of photons per area per pulse) are shown for both excitation wavelengths. The $\lambda^*=800$ nm excitation wavelength (Figure 3a) corresponds to an energy which is lower than twice the bandgap of the germanium NCs, so CM is energetically not possible. The experimental traces exhibit identical decay dynamics, with their amplitudes depending linearly on the excitation power (Supplementary Fig. S2). The inset shows the initial amplitude A (left hand scale) and the A/B ratio (right hand scale) for the transients as a function of the absorbed photon fluence. As expected, the initial magnitude of the transients, A, increases linearly with the number of absorbed photons. The observation that the ratio A/B is independent of the absorbed photon fluence demonstrates that the decay dynamics of the transients are invariant with changes of the pump laser fluence. This implies that an NC absorbs at most a single photon. We also note that the TA dynamics measured for the $\lambda^*=800$ nm excitation can be fitted with a single-exponential decay with the lifetime $\tau_1=3$ ns (dashed lines in Figure 3a) and features no fast component, which is consistent with the fact that no CM takes place for this energy.

Figure 3b shows the TA dynamics for the $\lambda^*=400$ nm excitation. As before, the transients are depicted at different pump fluences to demonstrate that the measurements are conducted in the regime in which an NC absorbs at most one photon (also see the inset and Supplementary Fig. S2). The traces can now be described by fitting a double-exponential to the data, as illustrated by the dashed lines with the lifetimes $\tau_1=3$ ns and $\tau_2=170$ ps. The additional fast component τ_2 is typical for Auger recombination in lead selenide NCs[38,41] and in silicon NCs in a silicon–dioxide matrix.[42] The occurrence of CM is confirmed by the higher A/B ratio as well as the steeper rise of the initial amplitude A upon increasing pump fluence for this short wavelength excitation.

Based on the results in Figure 3, we conclude that the exciton multiplicity at higher-energy excitations can be determined by fitting a double-exponential to the TA dynamics. Experimentally, the CM yield $\phi_{CM}(h\nu)$ is found from the A/B ratio scaled to the value measured for excitation at a low energy for which CM does not take place:

$$\phi_{CM}(h\nu)=\frac{A(h\nu)/B(h\nu)}{A(1.55\text{ eV})/B(1.55\text{ eV})} \tag{2}$$

To investigate the CM in detail, we have measured the exciton multiplicity in germanium NCs as a function of the excitation wavelength. The results are shown in Figure 5, which presents the number of e–h pairs created per absorbed photon determined as described above (all low fluence transients are available in Supplementary Fig. S3). This figure implies a CM efficiency of nearly 190% at 3.5 eV, i.e., 1.9 e–h pairs are created for each absorbed photon with energy 2.8 times the optical bandgap. The lower panel of the figure shows the PL spectrum and its mapped multiplicities ('2PL' and '3PL'). In the most favorable case, i.e., when CM would proceed in the energy conservation limit, the onset for multiplying carriers would appear at twice the PL energy, at which free carriers in some NCs have exactly enough excess energy to create a second e–h pair. We note that the onset for CM occurs at an energy which appears to be below two times the optical bandgap of germanium NCs, in this case 1.25 eV. This is because 1.25 eV represents the average energy gap of all the NCs present in the sample, and the experimentally measured onset will correspond to CM taking place in the largest NCs of the ensemble, which contains a distribution of bandgap energies. In summary, the

doi:10.1038/lsa.2015.24

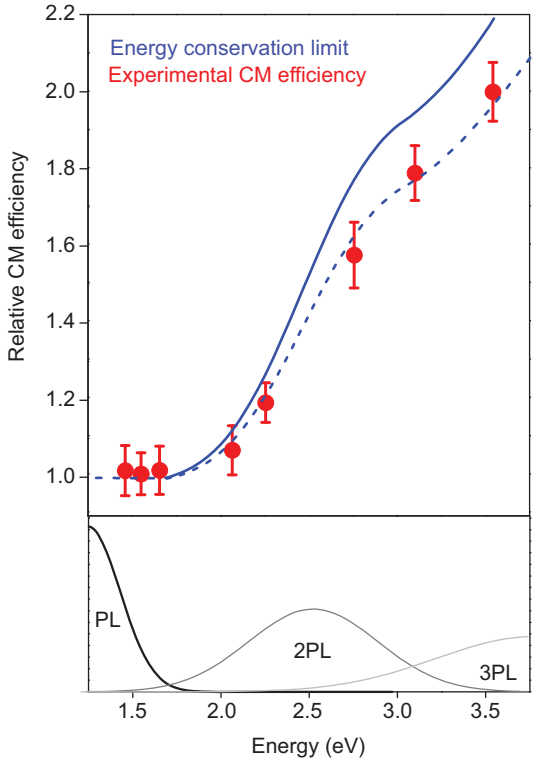

Figure 5 Relative CM efficiency (number of e–h pairs created per photon absorbed) as a function of the pump photon energy, based on the ratio of the fast and slow components of the TA transients. The bottom panel shows the PL spectrum and scaled multiples of it. The blue line is the energy conservation limit, which is the integral of the *n*PL curves (the dashed line is the integral scaled by a factor of 0.9 to coincide with the data points). CM, carrier multiplication; e–h, electron–hole; PL, photoluminescence; TA, transient absorption.

CM efficiency should follow the integral of the normalized *n*PL curves. The blue line in Figure 5 is the integral of *n*PL. The dashed trace corresponds to the same curve scaled by a factor of 0.9 to fit the data points. The quality of the fit supports the interpretation of the data discussed above. It is important to mention that in the present study we do not find any evidence of NC–NC interaction (as in our previous studies on silicon NCs[35,43]), and the reported effect concerns generation of multiple excitons in isolated germanium NCs.

A final question arises as to how the CM in the germanium NCs investigated in this study compares to CM in bulk germanium. For bulk germanium, Koc measured a CM efficiency of 170% for a photon energy of 4.15 eV, which corresponds to 6.2 times the bandgap.[10] In our measurements we observe 190% CM for an energy of 3.5 eV (2.8 times the bandgap of our germanium NCs). In bulk germanium, at 3.5 eV, the efficiency is only 140%, whereas this energy is 5.2 times the bandgap. We therefore conclude that CM is substantially more efficient in germanium NCs than in the bulk—both on the absolute energy scale and in comparison to the bandgap. This finding offers the prospect of a new generation of highly efficient infrared detectors and, perhaps, even solar cells based on germanium NCs.

CONCLUSIONS

We have shown the occurrence of CM in germanium NCs on the basis of measurements of the transient absorption as a function of the pump photon energy. The CM efficiency in germanium NCs was found to be considerably higher than in bulk germanium.

AUTHOR CONTRIBUTIONS

SS and TG conceived the project and designed the experiments; SS prepared the samples and performed experiments with CdW; SS analyzed the data; SS, PS and TG interpreted the data and co-wrote the manuscript; and FCMS, AJH and LDAS facilitated and interpreted the TA experiments and edited the manuscript. All authors discussed the results and the manuscript.

ACKNOWLEDGEMENTS

This work was financially supported by the Foundation for Fundamental Research on Matter (FOM).

1 Beard MC, Midgett AG, Hanna MC, Luther JM, Hughes BK *et al*. Comparing multiple exciton generation in quantum dots to impact ionization in bulk semiconductors: implications for enhancement of solar energy conversion. *Nano Lett* 2010; **10**: 3019–3027.
2 Nozik AJ. Nanoscience and nanostructures for photovoltaics and solar fuels. *Nano Lett* 2010; **10**: 2735–2741.
3 Beard MC, Luther JM, Semonin OE, Nozik AJ. Third generation photovoltaics based on multiple exciton generation in quantum confined semiconductors. *Accounts Chem Res* 2013; **46**: 1252–1260.
4 Nozik AJ. Quantum dot solar cells. *Physica E* 2002; **14**: 115–120.
5 Ellingson R. Solar cells: slicing and dicing photons. *Nat Photonics* 2008; **2**: 72–73.
6 Chaisakul P, Marris-Morini D, Frigerio J, Chrastina D, Rouifed MS *et al*. Integrated germanium optical interconnects on silicon substrates. *Nat Photonics* 2014; **8**: 482–488.
7 Semonin OE, Luther JM, Choi S, Chen HY, Gao J *et al*. Peak external photocurrent quantum efficiency exceeding 100% *via* MEG in a quantum dot solar cell. *Science* 2011; **334**: 1530–1533.
8 Kolodinski S, Werner JH, Wittchen T, Queisser HJ. Quantum efficiencies exceeding unity due to impact ionization in silicon solar cells. *Appl Phys Lett* 1993; **63**: 2405–2407.
9 Robbins DJ. Aspects of the theory of impact ionization in semiconductors (I). *Phys Status Solidi B* 1980; **97**: 9–50.
10 Koc S. The quantum efficiency of the photo-electric effect in germanium for the 0.3–2 μm wavelength region. *Czech J Phys* 1957; **7**: 91–95.
11 Tielrooij KJ, Song JC, Jensen SA, Centeno A, Pesquera A *et al*. Photoexcitation cascade and multiple hot-carrier generation in graphene. *Nat Phys* 2013; **9**: 248–252.
12 Aerts M, Bielewicz T, Klinke C, Grozema FC, Houtepen AJ *et al*. Highly efficient carrier multiplication in PbS nanosheets. *Nat Commun* 2014; **5**: 3789.
13 Gabor NM, Zhong Z, Bosnick K, Park J, McEuen PL. Extremely efficient multiple electron–hole pair generation in carbon nanotube photodiodes. *Science* 2009; **325**: 1367–1371.
14 Padilha LA, Stewart JT, Sandberg RL, Bae WK, Koh WK *et al*. Aspect ratio dependence of Auger recombination and carrier multiplication in PbSe nanorods. *Nano Lett* 2013; **13**: 1092–1099.
15 Cunningham PD, Boercker JE, Foos EE, Lumb MP, Smith AR *et al*. Enhanced multiple exciton generation in quasi-one-dimensional semiconductors. *Nano Lett* 2011; **11**: 3476–3481.
16 Smith C, Binks D. Multiple exciton generation in colloidal nanocrystals. *Nanomaterials* 2014; **4**: 19–45.
17 Ip AH, Thon SM, Hoogland S, Voznyy O, Zhitomirsky D *et al*. Hybrid passivated colloidal quantum dot solids. *Nat Nanotechnol* 2012; **7**: 577–582.
18 Ellingson RJ, Beard MC, Johnson JC, Yu P, Micic OI *et al*. Highly efficient multiple exciton generation in colloidal PbSe and PbS quantum dots. *Nano Lett* 2005; **5**: 865–871.
19 Midgett AG, Luther JM, Stewart JT, Smith DK, Padilha LA *et al*. Size and composition dependent multiple exciton generation efficiency in PbS, PbSe, and PbS_xSe_{1-x} alloyed quantum dots. *Nano Lett* 2013; **13**: 3078–3085.
20 Kim TY, Park NM, Kim KH, Sung GY, Ok YW *et al*. Quantum confinement effect of silicon nanocrystals *in situ* grown in silicon nitride films. *Appl Phys Lett* 2004; **85**: 5355–5357.
21 Priolo F, Gregorkiewicz T, Galli M, Krauss TF. Silicon nanostructures for photonics and photovoltaics. *Nat Nanotechnol* 2014; **9**: 19–32.
22 Michel J, Liu J, Kimerling LC. High-performance Ge-on-Si photodetectors. *Nat Photonics* 2010; **4**: 527–534.
23 Takeoka S, Fujii M, Hayashi S, Yamamoto K. Size-dependent near-infrared photoluminescence from Ge nanocrystals embedded in SiO_2 matrices. *Phys Rev B* 1998; **58**: 7921–7925.
24 Takeoka S, Toshikiyo K, Fujii M, Hayashi S, Yamamoto K. Photoluminescence from $Si_{1-x}Ge_x$ alloy nanocrystals. *Phys Rev B* 2000; **61**: 15988–15992.
25 Aerts M, Spoor FC, Grozema FC, Houtepen AJ, Schins JM *et al*. Cooling and Auger recombination of charges in PbSe nanorods: crossover from cubic to bimolecular decay. *Nano Lett* 2013; **13**: 4380–4386.
26 Barbagiovanni EG, Lockwood DJ, Simpson PJ, Goncharova LV. Quantum confinement in Si and Ge nanostructures. *J Appl Phys* 2012; **111**: 034307.

27 Bulutay C. Interband, intraband, and excited-state direct photon absorption of silicon and germanium nanocrystals embedded in a wide band-gap lattice. *Phys Rev B* 2007; **76**: 205321.
28 Niquet YM, Allan G, Delerue C, Lannoo M. Quantum confinement in germanium nanocrystals. *Appl Phys Lett* 2000; **77**: 1182–1184.
29 Cosentino S, Knebel S, Mirabella S, Gibilisco S, Simone F *et al*. Light absorption in Ge nanoclusters embedded in SiO_2: comparison between magnetron sputtering and sol–gel synthesis. *Appl Phys A* 2014; **116**: 233–241.
30 Saeed S, Buters F, Dohnalova K, Wosinski L, Gregorkiewicz T. Structural and optical characterization of self-assembled Ge nanocrystal layers grown by plasma-enhanced chemical vapor deposition. *Nanotechnology* 2014; **25**: 405705.
31 Richter H, Wang ZP, Ley L. The one phonon Raman spectrum in microcrystalline silicon. *Solid State Commun* 1981; **39**: 625–629.
32 Pinto SR, Rolo AG, Chahboun A, Kashtiban RJ, Bangert U *et al*. Raman study of stress effect on Ge nanocrystals embedded in Al_2O_3. *Thin Solid Films* 2010; **518**: 5378–5381.
33 Volodin VA, Marin DV, Sachkov VA, Gorokhov EB, Rinnert H *et al*. Applying an improved phonon confinement model to the analysis of Raman spectra of germanium nanocrystals. *J Exp Theor Phys* 2014; **118**: 65–71.
34 Trinh MT, Limpens R, de Boer WD, Schins JM, Siebbeles LD *et al*. Direct generation of multiple excitons in adjacent silicon nanocrystals revealed by induced absorption. *Nat Photonics* 2008; **6**: 316–321.
35 Tognini P, Stella A, Silvestri SD, Nisoli M, Stagira S *et al*. Ultrafast carrier dynamics in germanium nanoparticles. *Appl Phys Lett* 1999; **75**: 208–210.
36 Schaller RD, Sykora M, Pietryga JM, Klimov VI. Seven excitons at a cost of one: redefining the limits for conversion efficiency of photons into charge carriers. *Nano Lett* 2006; **6**: 424–429.
37 Trinh MT, Houtepen AJ, Schins JM, Hanrath T, Piris J *et al*. In spite of recent doubts carrier multiplication does occur in PbSe nanocrystals. *Nano Lett* 2008; **8**: 1713–1718.
38 Luther JM, Beard MC, Song Q, Law M, Ellingson RJ *et al*. Multiple exciton generation in films of electronically coupled PbSe quantum dots. *Nano Lett* 2007; **7**: 1779–1784.
39 Govoni M, Marri I, Ossicini S. Carrier multiplication between interacting nanocrystals for fostering silicon-based photovoltaics. *Nat Photonics* 2012; **6**: 672–679.
40 Marri I, Govoni M, Ossicini S. Red-shifted carrier multiplication energy threshold and exciton recycling mechanisms in strongly interacting silicon nanocrystals. *J Am Chem Soc* 2014; **136**: 13257–13266.
41 Beard MC, Midgett AG, Law M, Semonin OE, Ellingson RJ *et al*. Variations in the quantum efficiency of multiple exciton generation for a series of chemically treated PbSe nanocrystal films. *Nano Lett* 2009; **9**: 836–845.
42 Trinh MT, Limpens R, Gregorkiewicz T. Experimental investigations and modeling of Auger recombination in silicon nanocrystals. *J Phys Chem C* 2013; **117**: 5963–5968.
43 de Boer WD, Trinh MT, Timmerman D, Schins JM, Siebbeles LD *et al*. Increased carrier generation rate in Si nanocrystals in SiO_2 investigated by induced absorption. *Appl Phys Lett* 2011; **99**: 053126.

This work is licensed under a Creative Commons Attribution-NonCommercial-NoDerivs 3.0 Unported License. The images or other third party material in this article are included in the article's Creative Commons license, unless indicated otherwise in the credit line; if the material is not included under the Creative Commons license, users will need to obtain permission from the license holder to reproduce the material. To view a copy of this license, visit http://creativecommons.org/licenses/by-nc-nd/3.0/

Supplementary information for this article can be found on the *Light: Science & Applications*' website (http://www.nature.com/lsa/).